

Hidden Mott insulator in metallic PdCrO₂

Frank Lechermann

I. Institut für Theoretische Physik, Universität Hamburg, D-20355 Hamburg, Germany

There has been a long-standing debate on the coexistence between itinerant electrons and localized spins in the PdCrO₂ delafossite. By means of the charge self-consistent combination of density functional theory and dynamical mean-field theory, it is corroborated that despite overall remarkable metallic response, the CrO₂ layers are indeed Mott insulating. The resulting k -resolved spectral function in the paramagnetic phase is in excellent agreement with available photoemission data. Subtle coupling between the itinerant and Mott-localized degrees of freedom is revealed. Different doping scenarios are simulated in order to manipulate the electronic states within the inert layers. In particular, oxygen vacancies prove effective in turning the hidden Mott insulator into a strongly correlated itinerant subsystem. The present results may open a new venue in research on quantum materials beyond canonical classification schemes.

I. INTRODUCTION

The discrimination of distinct electronic phases is a standard paradigm in condensed matter physics. Fermi-liquid metals, band insulators and Mott insulators form the canonical ones. Several doped Mott insulators, for instance, belong to a more complex class, but still, material characterization usually focuses on the global aspects given by transport and magnetism. Recently, oxide heterostructures challenged this viewpoint, by establishing rather different electronic states in selected real-space regions in a controlled way. There, e.g. conducting interface regions are replaced by highly Mott-insulating areas further away from the interface¹⁻³. The question arises if such coexistence of itinerancy and Mott localization can also be found in natural materials.

In that respect, the delafossite compound PdCrO₂^{4,5} provides an intriguing test case. Selected ABO₂ delafossites⁶, where A and B are different transition-metal (TM) atoms, such as PdCoO₂, PtCoO₂ and PdCrO₂ are surprisingly high conductive (see e.g. Refs. 7 and 8 for recent reviews). The room-temperature inplane resistivity of PdCoO₂ amounts to 2.6 $\mu\Omega\text{cm}$ ⁹, rendering it the most-conductive oxide in this temperature (T) range. The crystal structure displayed in Fig. 1 shows the delafossite stacking of triangular A -atom planes and trigonal BO₂ planes along the c -axis exemplified for PdCrO₂. As a key fact, the TM environments strongly differ for A and B sites. The B sites are in a common trigonal-oxide placing, giving rise to d -shell states of $t_{2g} = \{a_{1g}, e'_g\}$ character at low energy and of e_g nature at high energy. On the other hand, the A sites are linked to apical oxygens up and below, eventually leading to a more unusual d -state hierarchy. Experiments hint towards rather inert BO₂ layers in terms of itinerancy. From a general formal-oxidation analysis, the valences $A^{+1}B^{3+}O_2^{2-}$ describe cobalt in (Pd,Pt)CoO₂ compounds as $\text{Co}^{3+}(3d^6)$ with a low-spin closed- t_{2g} subshell structure. This resembles the Co state in related NaCoO₂, the band-insulating layered rock salt¹⁰ with both Na and Co in a trigonal position. Though already the interplay between the itinerant $4d$ electrons and the inert $3d^6$ configuration of cobalt

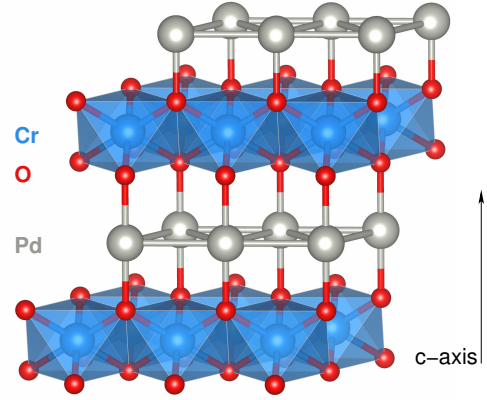


FIG. 1. (color online) Delafossite ABO₂ crystal structure exemplified for PdCrO₂ with Pd (grey), Cr (blue) and O (red).

raises interesting questions, the case of PdCrO₂ appears even more intriguing. Formal low-spin $\text{Cr}^{3+}(3d^3)$ has a half-filled t_{2g} shell, with expected sizable local Coulomb interaction. Mott criticality in the CrO₂ layers becomes possible and several experiments indeed hint towards localized Cr^{3+} spins^{4,11} in contact with itinerant Pd($4d$) electrons. Furthermore, magnetic ordering in a 120° spin structure is confirmed below $T_N = 37.5$ K.

In this work, a detailed study of the correlated electronic structure of paramagnetic PdCrO₂ is presented, revealing the Mott-insulating character of the CrO₂ layers from first-principles many-body theory. Due to its concealed nature in the overall very good metallic system, one may classify this real-space-selective insulating regime as a 'hidden Mott insulator'. The k -resolved interacting spectral function differs substantially from the effective single-particle band structure obtained within conventional density functional theory (DFT). As the spectral weight of low-energy Cr-like DFT bands is shifted to higher energies with correlations, the Fermi level gets positioned in a one-band Pd-dominated quasi-particle (QP) dispersion. Significant coupling between the localized Cr electrons and the itinerant Pd electrons

is discovered from analyzing the electronic self-energy. Different doping scenarios are employed to perturb the hidden state, eventually rendering the CrO_2 layers itinerant.

II. THEORETICAL APPROACH

The charge self-consistent combination of density functional theory and dynamical mean-field theory (DMFT) is employed^{12–14}. For the DFT part, I use the mixed-basis pseudopotential method^{15,16}, based on norm-conserving pseudopotentials with a combined basis of localized functions and plane waves. For the exchange-correlation part in DFT, the generalized-gradient approximation in form of the PBE functional¹⁷ is utilized. Within the mixed basis, localized functions for $\text{Cr}(3d)$ and $\text{Pd}(4d)$ states as well as for $\text{O}(2s)$ and $\text{O}(2p)$ are used in order to reduce the plane-wave energy cutoff. The correlated subspace consists of the effective $\text{Cr}(3d)$ Wannier-like functions as obtained from the projected-local-orbital formalism^{18,19}, using as projection functions the linear combinations of atomic $3d$ orbitals, diagonalizing the $\text{Cr}(3d)$ orbital-density matrix. I use a five-orbital Slater-Kanamori Hubbard Hamiltonian in the correlated subspace, parametrized by a Hubbard $U = 3\text{eV}$ and a Hund's exchange $J_H = 0.7\text{eV}$. The latter values represent a proper choice for chromium oxides²⁰ and for akin layered CoO_2 compounds²¹. Since the relevant d -states of palladium are of $4d$ character and are furthermore close to complete filling in PdCrO_2 , the effect of explicit local Coulomb interactions on the Pd site may be safely neglected for examining the qualitative key physics. The single-site DMFT impurity problems in stoichiometric and doped PdCrO_2 are solved by the continuous-time quantum Monte Carlo scheme^{22,23} as implemented in the TRIQS package^{24,25}. A double-counting correction of fully-localized type²⁶ is applied. To obtain the spectral information, analytical continuation from Matsubara space via the maximum-entropy method as well as the Padé method is performed. All DFT+DMFT calculations are conducted by setting the system temperature to $T = 290\text{K}$. Paramagnetism is assumed in all those computations.

Experimental lattice parameters⁶ $a = 2.930\text{Å}$ and $c = 18.097\text{Å}$ are used. The internal degree of freedom z , governing the oxygen distance to the Pd plane is obtained from DFT structural optimization, reading $z = 0.1101$ for the stoichiometric compound.

III. RESULTS

A. DFT electronic structure

Within Kohn-Sham density functional theory, the main results of characterizing nonmagnetic PdCrO_2 are

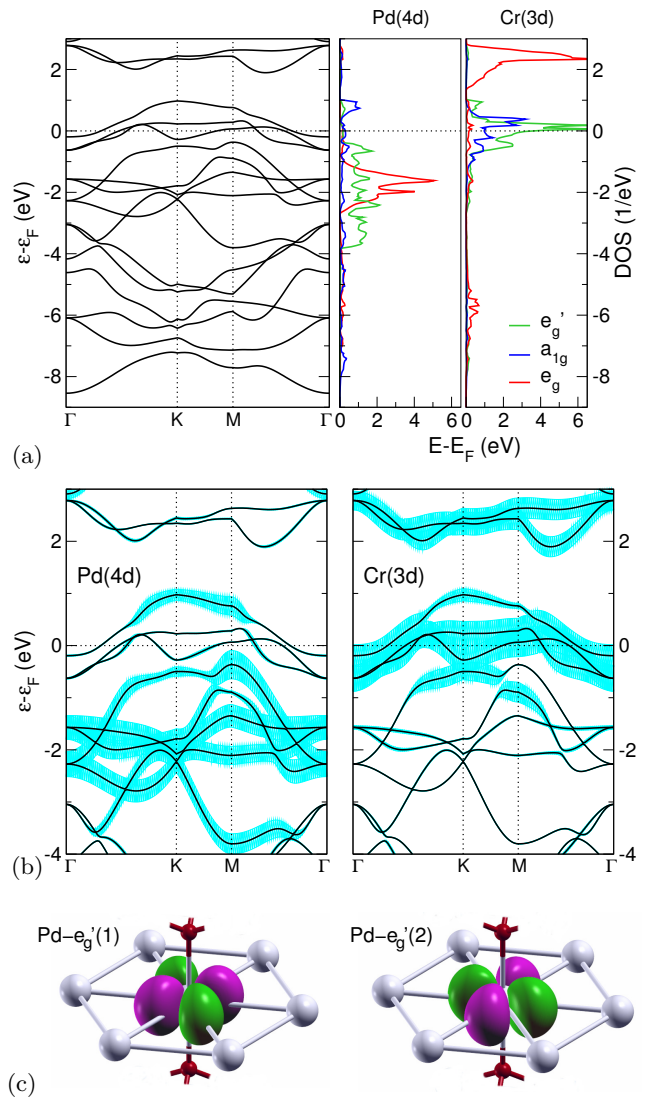


FIG. 2. (color online) Bandstructure and density of states (DOS) from DFT. (a) Bands within the $k_z = 0$ plane along high-symmetry directions (left) and local density of states for Pd and Cr (right). Note that the $\text{Pd-}a_{1g}$ orbital points towards the apical oxygen and the $\text{Pd-}e'_g$ marks strictly inplane orbitals. (b) $\text{Pd}(4d)$ (left) and $\text{Cr}(3d)$ (right) character on the TM-dominated bands. (c) In-plane $\text{Pd-}e'_g$ orbitals, dominating the band just below the low-energy $\text{Cr-}t_{2g}$ manifold.

displayed in Fig. 2. The relevant band structure and density of states (DOS) encompassing $\text{Pd}(4d)$, $\text{Cr}(3d)$ and $\text{O}(2p)$ states spans an energy window of $[-8.5, 3]\text{eV}$ (cf. Fig. 2a). The Cr levels are higher in energy than the Pd ones, rendering the latter not too far from complete filling. At the Fermi level, a separated manifold of three bands marks a dispersion of width 1.6eV. These bands are nearly exclusively of $\text{Cr}(3d)$ character as also visible from the 'fatband' plot of Fig. 2b, which visualizes the underlying $\text{Pd}(4d)$ and $\text{Cr}(3d)$ contribution to each band. In more detail, from the trigonal splitting at the Cr site,

the given low-energy bands are dominantly of t_{2g} kind, consisting of a_{1g} and doubly-degenerate e'_g orbitals. Note that the Cr- a_{1g} orbital points along the c -axis, while the Cr- e'_g orbitals point in direction between the oxygen ligands and are inclined to the vertical axis. The remaining Cr- e_g orbitals of higher energy are directed towards the oxygens. Because of the different site symmetry, the Pd- a_{1g} orbital points to the apical oxygens and therefore does not mark a low-energy orbital as in the Cr case.

Remarkably, the just described DFT-based low-energy electronic structure disagrees completely with angle-resolved photoemission spectroscopy (ARPES) experiments^{11,27}. There, only a single QP band crosses the Fermi level, which also from quantum-oscillation experiments^{28,29} is designated as being dominantly of Pd character. The obvious solution to this discrepancy is given by the fact that the Cr states are effectively localized due to electronic correlations based on sizable local Coulomb interactions. In other words, the CrO₂ layers become Mott insulating, while the Fermi level of the still overall metallic system shifts into a Pd-dominated QP band. From Fig. 2b, it appears obvious to which principle band it comes down to: the band just below the Cr-based low-energy threefold of bands, which is of strong Pd($4d$) character, has to take charge. Importantly, that band carries dominantly Pd- e'_g weight (cf. Fig. 2a,b), which represents a twofold of in-plane orbitals (see Fig. 2c). In the following, I will call this band the 'conducting Pd (cPd) band'. Note that Pd adds also some angular-momentum contribution from s and p over the relevant energy range, but the corresponding magnitude is always about 5-10 times smaller than from d flavour.

Regarding the general spectral properties, some agreement with experiment can be achieved within spin-polarized DFT calculations for a magnetically ordered system^{11,27,30,31}. However in the next section it will be shown that agreement with experiment is not truly associated with invoking magnetic order, but by correctly including the physics of generic electron correlations beyond conventional DFT.

B. Correlated electronic structure of PdCrO₂

1. Main spectral properties

Figure 3 summarizes the spectral information that is obtained with charge self-consistent DFT+DMFT. The k -resolved spectral function $A(\mathbf{k}, \omega)$ plotted in Fig. 3a along high-symmetry lines in the $k_z = 0$ plane of reciprocal space exhibits the expected matching with experimental findings. A single QP band crosses the Fermi energy ε_F along Γ - K and Γ - M . Comparison of the band labelling with the original DFT bandstructure easily verifies it as indeed stemming dominantly from the cPd band. The Fermi wavevector with a fraction of 0.61 along the complete Γ - K path, as well as the central-peak energy of -0.29 eV of the occupied hole pocket at the M -point are

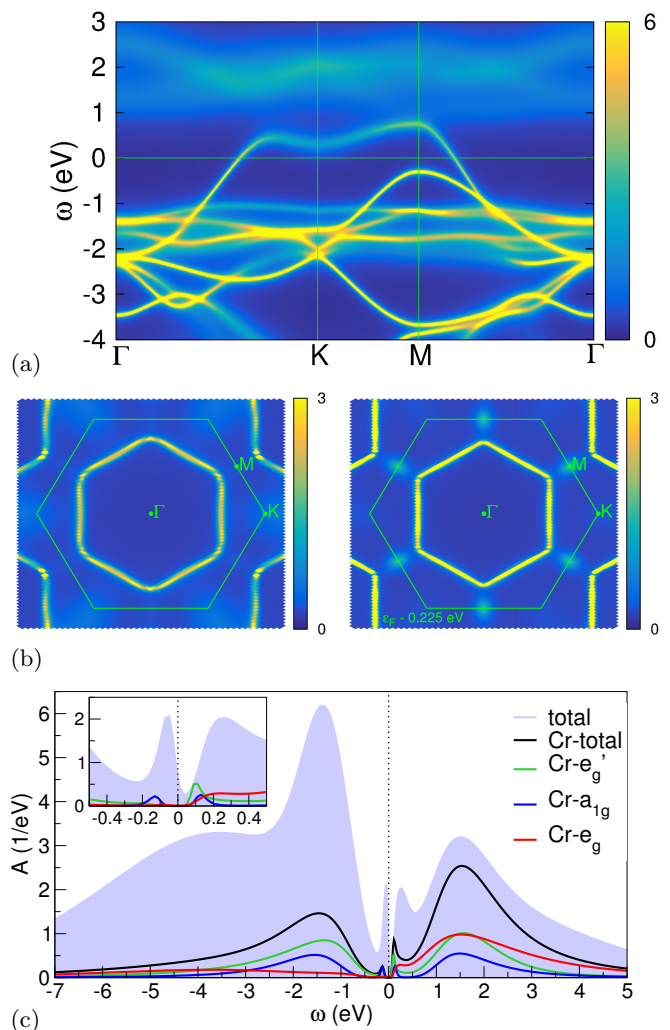


FIG. 3. (color online) Spectral data from DFT+DMFT. (a) Spectral function $A(\mathbf{k}, \omega)$ along high-symmetry lines in the $k_z = 0$ plane of reciprocal space. (b) Constant-energy surfaces within the first Brillouin zone (green hexagon): Fermi surface $\omega = \varepsilon_F = 0$ (left) and $\omega = \varepsilon_F - 0.225$ eV. (c) k -integrated spectral function $A(\omega)$ with orbital-resolved local Cr part. Inset: blow-up around Fermi level.

in very good agreement with ARPES data^{11,27}. While the occupied Pd bands away from the Fermi level show mostly proper coherency, the original Cr- e_g bands above ε_F are now strongly incoherent. Importantly, the former Cr- t_{2g} bands at low-energy have fully disintegrated. The Fermi surface in Fig. 3b agrees with the single-sheet hexagon centered around Γ from experiment²⁷, and also the constant-energy cut somewhat below ε_F reveals again the same pocket structure around the symmetry-equivalent M -points.

Of course, the Cr spectral weight has not vanished into thin air. As shown from a plot of the k -integrated total spectral function and the local chromium part in Fig. 3c, the Cr spectral weight is broadly distributed over energies away from the Fermi level, with dispersive parts mingling

with the Pd bands. Right at ε_F there is zero spectral weight, i.e. Cr is charge gapped and the CrO_2 layer indeed Mott insulating. Due to the overall metallicity of the system, this may be called a 'hidden Mott insulator' in a real-space selective region of the material. From theory, such Mott states in itinerant systems have e.g. already be found in oxide heterostructures^{2,3}. The 'lower Hubbard band' of hidden-Mott Cr extends over the Pd-dominated energy region and becomes therefore rather invisible as a distinct excitation in $A(\mathbf{k}, \omega)$ (cf. Fig. 3a). The orbital-resolved Cr occupations from DFT+DMFT read $n = \{n_{e'_g}, n_{a_{1g}}, n_{e_g}\} = \{2.07, 1.02, 1.06\}$ with a total electron count of $n_{\text{tot}} = 4.15$. At first glance, this seems to disagree with the straightforward picture of Cr^{3+} with spin $S = 3/2$ that is usually put forward from basic considerations. However note that the Wannier-based Cr- e_g spectral weight of one electron is very flat in the occupied region, marking the broad hybridization with its surrounding. Thus, the more localized t_{2g} electrons shall count most when it comes to local properties and therefrom Cr^{3+} with $S = S_{t_{2g}} \approx 3/2$ indeed matches expectations. In this respect, note that Pd is nominally in the '+1' oxidation state, which is usually interpreted as a $4d^9$ configuration.

2. Coupling of localized and itinerant electrons

So far, the advanced electronic structure theory beyond DFT was mainly utilized to achieve agreement with available experimental findings. However, it reveals also important new insight into the crucial coupling of itinerant electrons with dominant Pd character and localized Cr electrons^{28,32}.

Traditionally, such couplings are known from Kondo physics, namely in an incoherent way associated with a Kondo impurity and in the coherent way on a Kondo lattice. The latter may applies to heavy-fermion compounds, where a regular lattice of localized f -electron spins interacts with a surrounding Fermi sea^{33,34}. Key competition in such a system is between the antiferromagnetic Rudermann-Kittel-Kasuya-Yosida (RKKY) interaction trying to order the spins and the Kondo effect trying to screen the spins. Seemingly, the present PdCrO_2 problem exhibits some similarities to the basic architecture of the Kondo-lattice problem, but importantly, the present localized spins do not result from atomic physics of partially-filled inner f -shells. Instead, the Cr spins originate from a Mott mechanism that suppresses the hopping via strong local Coulomb repulsion. Little formal details are known about this regime of itinerant-localized electron coupling.

As already shown in Fig. 3c, there is some minor Cr spectral weight appearing at low energy close to ε_F , which is a hint for a coupling to the itinerant Pd electrons. Furthermore on the DFT level, it is there is substantial Cr($3d$) weight on the cPd band around the K -point (see Fig. 2b). It is therefore expected that the itin-

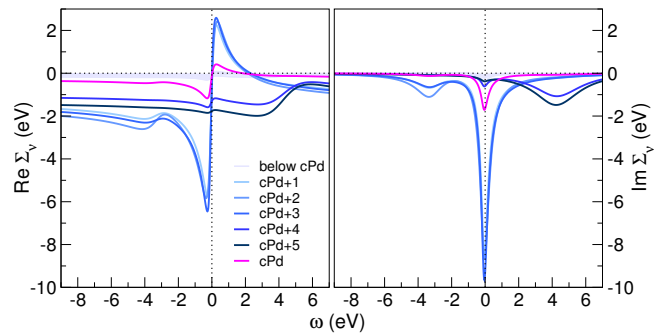


FIG. 4. (color online) Diagonal elements of the two-dimensional self-energy $\Sigma_{\nu\nu'}^{2D}(\omega)$ in the band basis. Left: real part, right: imaginary part. The self-energy on the cPd band is highlighted (magenta).

erant Pd electrons carry some self-energy (or 'heaviness') from scattering with the highly correlated Cr electrons. This can be made quantitative via the self-energy expression in the Bloch basis $\{|\mathbf{k}\nu\rangle\}$, reading¹⁸

$$\Sigma_{\nu\nu'}(\mathbf{k}, \omega) = \sum_{\mathbf{R}, mm'} \bar{P}_{\nu m}^{\mathbf{R}*}(\mathbf{k}) (\Sigma_{mm'}^{\mathbf{R}}(\omega) - \Sigma^{\text{dc}}) \bar{P}_{m'\nu'}^{\mathbf{R}}(\mathbf{k}), \quad (1)$$

whereby here, $\nu\nu'$ are band indices, mm' denote Cr($3d$) states, \mathbf{R} are Cr sites and \bar{P} are the projections between Bloch and local space. The local self-energy correction to DFT on a given Cr site is given by the difference between the DMFT impurity self-energy $\Sigma_{mm'}^{\mathbf{R}}(\omega)$ and the double-counting term Σ^{dc} . For the key effects, one may restrict the discussion to inplane correlations, since most electron-electron scattering will happen in the relevant twodimensional (2D) subspace of the layered material. Figure 4 displays real and imaginary part of the self-energy $\Sigma_{\nu\nu'}^{2D}(\omega)$, representing the diagonal elements of the k -summed $\Sigma_{\nu\nu'}(\mathbf{k}, \omega)$ with $k_z = 0$. Besides the expected large self-energy on the Cr-dominated bands, there is also a sizable self-energy amplitude on the cPd band. On the contrary, for the bands further below in energy, $\Sigma_{\nu\nu'}^{2D}(\omega)$ turns out very small.

In other words, albeit no explicit local Coulomb repulsion is taken into account within DFT+DMFT on the Pd sites, the scattering with Mott-localized Cr electrons transfers some correlations onto the most-relevant Pd-dominated band. This will not only effect the transport properties^{35,36} but also the exchange interaction between the Cr spins. Due to the half-filled scenario of the Cr($3d$) sites, kinetic exchange of antiferromagnetic kind is most natural. The revealed *additional* coupling to the itinerant Pd electrons could cause an RKKY-like contribution. Understanding the intricate PdCrO_2 magnetism^{4,5,31,36-38}, which should be also partly rooted in the frustration on the triangular Cr sublattice, will ask for a detailed assessment of the different exchange contributions.

C. Doping effects

The question arises, if the hidden Mott-insulating state in PdCrO₂ could be perturbed such that the correlation physics emerges more blatantly, perhaps triggering other interesting physics. Various doped Mott insulators serve as prominent examples for the latter, and thus doping may provoke new phenomena in the given delafossite. For instance, from basic considerations, electron- or hole-doped Cr sites might give rise to additional low-energy QP(-like) states.

From the viewpoint of theory engineering, two ways of doping are feasible. First, through a perfectly-coherent charge doping by making use of the virtual-crystal approximation (VCA). A selected atomic species is thereby replaced by a pseudo atom of different nuclear charge $Z \pm \delta$. Second, and more realistic to experimental capabilities, through the introduction of explicit defects in a supercell approach.

1. Coherent hole doping

Let's first deal with the somewhat more exemplary, but computationally simpler, coherent doping within VCA. For a proof of principles, I focus on introducing holes via

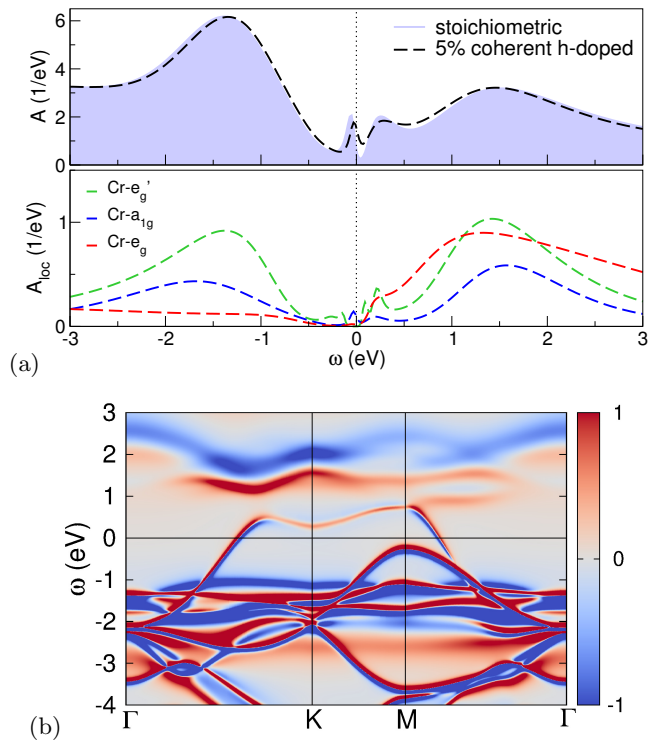


FIG. 5. (color online) Electronic spectrum of PdCrO₂ with coherent doping of 5% holes. (a) Integrated spectral functions, total (top) and local Cr (bottom). (b) Difference between the hole-doped angle-resolved spectrum and the stoichiometric one, i.e. $A_{\text{h-doped}}(\mathbf{k}, \omega) - A_{\text{undoped}}(\mathbf{k}, \omega)$.

doping	Cr- e'_g	Cr- a_{1g}	Cr- e_g	total
stoichiometric	2.07	1.02	1.06	4.15
coherent 5% holes	2.09	1.03	1.10	4.22
O vacancy	2.12	1.05	1.45	4.62
Pd vacancy	2.06	1.02	1.15	4.23

TABLE I. Orbital-resolved Cr(3d) occupations. For the explicit-defect cases, averaging over all Cr sites in the supercell, respectively, is performed.

pseudizing Cr with a charge modification $\delta = 0.05$, resembling 5% hole doping in terms of doped carriers per correlated site. Upon structural relaxation, the z parameter of the crystal structure remains essentially unmodified with respect to the stoichiometric case.

As expected, the small hole doping leads to a shift of the electronic spectrum, placing the maximum of the total QP peak even closer to ε_F (see Fig. 5a). In addition, some low-energy spectral weight emerges from the CrO₂ layers, rendering the original hidden Mott insulator weakly metallic. Non-surprisingly, the Cr- a_{1g} orbital which points to the itinerant Pd layer generates the largest contribution at the Fermi level. Comparing the angle-resolved spectrum in Fig. 5b with the one at stoichiometry shows, that the cPd quasiparticle band also shifts as expected. However, due to the small doping and the coherent scenario, neglecting local structural distortions and symmetry breakings, the overall impact on the electronic spectrum remains without dramatic consequences. Interestingly, the original introduction of holes on the Cr sites on the atomic level, i.e. when initializing the calculation, results at DFT+DMFT convergence in a slightly *larger* nominal Cr(3d) charge (cf. Tab. I). Thus screening charge flow from nearby oxygens and/or the Pd layer overcompensates the initial Cr holes.

2. Doping by vacancies of oxygen or palladium type

Doping closer to common experimental procedures may be realized by introducing explicit defects in the system. I here choose vacancies of oxygen (O_V) and Pd (Pd_V) type to proceed along these lines. For both doping cases, 2×2×1 supercells are constructed with structural optimization of the atomic positions. Both defect structures shelter 4 inplane Pd, 4 inplane Cr and 8 O sites, respectively. While the O_V disturbs the participating CrO₆ octahedra and drags the Pd ion above towards the CrO₂ plane, the Pd_V pulls the respective O ions above and below towards the Pd plane and thereby distorts the corresponding CrO₆ octahedra. The present doping of 12.5% O_Vs and of 25% Pd_Vs is rather large, but suits the goal to study principle effects.

The main spectral properties are summarized in Fig. 6. Both doping scenarios lead to an enhancement of the low-energy QP peak in the total spectral function, which is

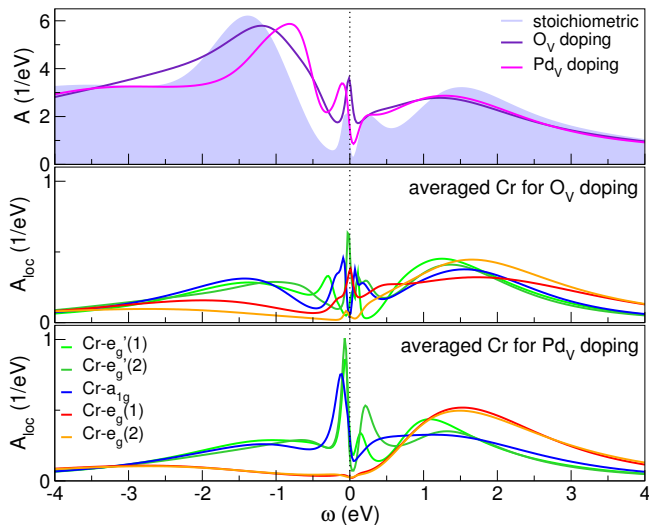


FIG. 6. (color online) Spectral properties of the O_V -doped and Pd_V -doped cases. Top: comparison of total spectral functions to stoichiometric case. Middle: Averaged Cr local spectral function for O_V doping. Bottom: Averaged Cr local spectral function for Pd_V doping.

obviously connected to the 'activation' of the originally transport-inert CrO_2 planes. Indeed, the averaged local Cr spectra now show sizable weight close to ε_F . Importantly, whereas in the previous case of coherent doping only the impact of charge alteration took place, here, additional factors come into play. Besides the different total electronic charge from taking out one O/Pd atom, the local symmetry breaking and structural distortions caused by this operation are also crucial for the doping aspects. Concerning the charge doping on the Cr site, the orbital-resolved occupation of the $Cr(3d)$ states are given in Tab. I. As expected for early TM oxides^{39–42}, introducing O_V s dominantly adds charge to the $TM-e_g$ states, resulting here in a significantly larger nominal Cr charge. The associated $Cr-e_g(1)$ state (that is connected to the vacant O site) develops furthermore sizable low-energy weight. On the other hand, the Pd_V has only minor effects on the $Cr(3d)$ filling, with also a slight increase in the $Cr-e_g$ electron count.

In comparison, the differences in charge doping of the $Cr-t_{2g}$ states between coherent and impurity doping are rather small. The still much larger response in the latter case points to relevant doping contributions from distortions and symmetry changes. In the case of doping with oxygen vacancies, the Cr-based QP resonances at the Fermi level are sharp and the rather particle-hole symmetric local spectrum is reminiscent of a canonical strongly correlated system close to half-filled Mott criticality⁴³ (cf. Fig. 6, middle). Apparently, Pd_V doping tends to reduce the correlation strength in the CrO_2 planes by even stronger means (here also because of the larger nominal doping level). The local Cr spectral func-

tion with 25% Pd_V s has an appearance similar to a moderately correlated $TM-t_{2g}$ oxide⁴⁴.

IV. CONCLUSIONS

A detailed investigation of the correlated electronic structure of highly-conductive $PdCrO_2$ revealed the hidden Mott insulator within the CrO_2 layers. The intriguing coexistence of a moderately correlated low-energy band and strongly correlated localized states renders the given material highly interesting, standing out of the large class of correlated TM oxides. Charge self-consistent DFT+DMFT is a proper tool to characterize the challenging electronic system, providing very good agreement with available spectral data from experiment. The low-energy QP band observed in ARPES measurements is of dominant $Pd(4d)$ character, carrying subtle correlation effects from the coupling to the localized $Cr(3d)$ states. Impurity doping proves effective in 'melting' the hidden Mott insulator, giving rise to intricate conductive correlated states. Here, it was shown that in particular oxygen vacancies may be suitable to generate demanding correlated transport. Notably, besides the sole carrier-doping impact, the effects of symmetry breaking and structural distortion appear also very important for the doping aspect.

Albeit so far, nearly exclusively, experimental studies of $PdCrO_2$ focussed on the high-purity aspect and the magnetic properties at stoichiometry, additional work on doped $PdCrO_2$ would be very interesting⁴⁵. There is the chance for identifying exciting electronic instabilities beyond the known low-temperature antiferromagnetic(-like) order at stoichiometry. The present work dealt with the paramagnetic electronic structure at room temperature. A theoretical study of the magnetic degrees of freedom, including e.g. a computation of exchange interactions, will be addressed in subsequent work. Moreover, revealing the T -dependent multi-orbital lattice susceptibilities from a realistic many-body perspective within DFT+DMFT⁴⁶ could shed further light on the intriguing electronic couplings in the system.

Finally, the $PdCrO_2$ compound (and also other delafosites) might be a promising candidate as a building block for novel oxide heterostructures with underlying triangular lattices. The unique layered structure and sensitivity to doping could open the possibility for engineering exceptional transport properties.

ACKNOWLEDGMENTS

Financial support from the DFG LE-2446/4-1 project "Design of strongly correlated materials" is acknowledged. Computations were performed at the JURECA Cluster of the Jülich Supercomputing Centre (JSC) under project number hhh08.

- ¹ C. A. Jackson, J. Y. Zhang, C. R. Freeze, and S. Stemmer, *Nat. Commun.* **5**, 4258 (2014).
- ² F. Lechermann and M. Obermeyer, *New J. Phys.* **17**, 043026 (2015).
- ³ F. Lechermann, *Sci. Rep.* **7**, 1565 (2017).
- ⁴ H. Takatsu, H. Yoshizawa, S. Yonezawa, and Y. Maeno, *Phys. Rev. B* **79**, 104424 (2009).
- ⁵ H. Takatsu, S. Yonezawa, C. Michioka, K. Yoshimura, and Y. Maeno, *J. Phys. Conf. Ser.* **200**, 012198 (2010).
- ⁶ R. D. Shannon, D. B. Rogers, and C. T. Prewitt, *Inorg. Chem.* **10**, 713 (1971).
C. T. Prewitt, R. D. Shannon, and D. B. Rogers, *Inorg. Chem.* **10**, 719 (1971).
D. B. Rogers, R. D. Shannon, and C. T. Prewitt, *Inorg. Chem.* **10**, 723 (1971).
- ⁷ A. P. Mackenzie, *Rep. Prog. Phys.* **80**, 032501 (2017).
- ⁸ R. Daou, R. Frésard, V. Eyert, S. Hébert, and A. Maignan, *Science and Technology of Advanced Materials* **18**, 919 (2017).
- ⁹ C. W. Hicks, A. S. Gibbs, A. P. Mackenzie, H. Takatsu, Y. Maeno, and E. A. Yelland, *Phys. Rev. Lett.* **109**, 116401 (2012).
- ¹⁰ Y. Takahashi, Y. Gotoha, and J. Akimoto, *J. of Solid State Chem.* **172**, 22 (2003).
- ¹¹ H.-J. Noh, J. Jeong, B. Chang, D. Jeong, H. S. Moon, E.-J. Cho, J. M. Ok, J. S. Kim, K. Kim, B. I. Min, et al., *Sci. Rep.* **4**, 3680 (2014).
- ¹² S. Y. Savrasov, G. Kotliar, and E. Abrahams, *Nature* **410**, 793 (2001).
- ¹³ L. V. Pourovskii, B. Amadon, S. Biermann, and A. Georges, *Phys. Rev. B* **76**, 235101 (2007).
- ¹⁴ D. Grieger, C. Piefke, O. E. Peil, and F. Lechermann, *Phys. Rev. B* **86**, 155121 (2012).
- ¹⁵ S. G. Louie, K. M. Ho, and M. L. Cohen, *Phys. Rev. B* **19**, 1774 (1979).
- ¹⁶ B. Meyer, C. Elsässer, F. Lechermann, and M. Fähnle, *FORTRAN 90 Program for Mixed-Basis-Pseudopotential Calculations for Crystals*, Max-Planck-Institut für Metallforschung, Stuttgart (1998).
- ¹⁷ J. P. Perdew, K. Burke, and M. Ernzerhof, *Phys. Rev. Lett.* **77**, 3865 (1996).
- ¹⁸ B. Amadon, F. Lechermann, A. Georges, F. Jollet, T. O. Wehling, and A. I. Lichtenstein, *Phys. Rev. B* **77**, 205112 (2008).
- ¹⁹ V. I. Anisimov, D. E. Kondakov, A. V. Kozhevnikov, I. A. Nekrasov, Z. V. Pchelkina, J. W. Allen, S.-K. Mo, H.-D. Kim, P. Metcalf, S. Suga, et al., *Phys. Rev. B* **71**, 125119 (2005).
- ²⁰ M. A. Korotin, V. I. Anisimov, D. I. Khomskii, and G. A. Sawatzky, *Phys. Rev. Lett.* **80**, 4305 (1998).
- ²¹ F. Lechermann, *Phys. Rev. Lett.* **102**, 046403 (2009).
- ²² A. N. Rubtsov, V. V. Savkin, and A. I. Lichtenstein, *Phys. Rev. B* **72**, 035122 (2005).
- ²³ P. Werner, A. Comanac, L. de' Medici, M. Troyer, and A. J. Millis, *Phys. Rev. Lett.* **97**, 076405 (2006).
- ²⁴ O. Parcollet, M. Ferrero, T. Ayril, H. Hafermann, I. Krivenko, L. Messio, and P. Seth, *Comput. Phys. Commun.* **196**, 398 (2015).
- ²⁵ P. Seth, I. Krivenko, M. Ferrero, and O. Parcollet, *Comput. Phys. Commun.* **200**, 274 (2016).
- ²⁶ V. I. Anisimov, I. V. Solovyev, M. A. Korotin, M. T. Czyżyk, and G. A. Sawatzky, *Phys. Rev. B* **48**, 16929 (1993).
- ²⁷ J. A. Sobota, K. Kim, H. Takatsu, M. Hashimoto, S.-K. Mo, Z. Hussain, T. Oguchi, T. Shishidou, Y. Maeno, B. I. Min, et al., *Phys. Rev. B* **88**, 125109 (2013).
- ²⁸ J. M. Ok, Y. J. Jo, K. Kim, T. Shishidou, E. S. Choi, H.-J. Noh, T. Oguchi, B. I. Min, , and J. S. Kim, *Phys. Rev. Lett.* **111**, 176405 (2013).
- ²⁹ C. W. Hicks, A. S. Gibbs, L. Zhao, P. Kushwaha, H. Borrmann, A. P. Mackenzie, H. Takatsu, S. Yonezawa, Y. Maeno, and E. A. Yelland, *Phys. Rev. B* **92**, 014425 (2015).
- ³⁰ K. P. Ong and D. J. Singh, *Phys. Rev. B* **85**, 134403 (2012).
- ³¹ D. Billington, D. Ernstring, T. E. Millichamp, C. Lester, S. B. Dugdale, D. Kersh, J. A. Duffy, S. R. Giblin, J. W. Taylor, P. Manuel, et al., *Sci. Rep.* **5**, 12428 (2015).
- ³² A. Glamazda, W.-J. Lee, S.-H. Do, K.-Y. Choi, P. Lemmens, J. van Tol, J. Jeong, and H.-J. Noh, *Phys. Rev. B* **90**, 045122 (2014).
- ³³ N. Mott, *Philosophical Magazine* **30**, 403 (1974).
- ³⁴ S. Doniach, *Physica B* **91**, 231 (1977).
- ³⁵ R. Daou, R. Frésard, S. Hébert, and A. Maignan, *Phys. Rev. B* **92**, 245115 (2015).
- ³⁶ S. Arsenijević, J. M. Ok, P. Robinson, S. Ghannadzadeh, M. I. Katsnelson, J. S. Kim, , and N. E. Hussey, *Phys. Rev. Lett.* **116**, 087202 (2016).
- ³⁷ S. Ghannadzadeh, S. Licciardello, S. Arsenijević, P. Robinson, H. Takatsu, M. I. Katsnelson, and N. E. Hussey, *Nat. Commun.* **8**, 15001 (2017).
- ³⁸ M. D. Le, S. Jeon, A. I. Kolesnikov, D. J. Voneshen, A. S. Gibbs, J. S. Kim, J. Jeong, H.-J. Noh, C. Park, J. Yu, et al., arXiv:1804.05573 (2018).
- ³⁹ W. Luo, W. Duan, S. G. Louie, and M. L. Cohen, *Phys. Rev. B* **70**, 214109 (2004).
- ⁴⁰ C. Mitra, C. Lin, J. Robertson, and A. A. Demkov, *Phys. Rev. B* **86**, 155105 (2012).
- ⁴¹ N. Pavlenko, T. Kopp, E. Y. Tsymbal, J. Mannhart, and G. A. Sawatzky, *Phys. Rev. B* **86**, 064431 (2012).
- ⁴² F. Lechermann, H. O. Jeschke, A. J. Kim, S. Backes, and R. Valentí, *Phys. Rev. B* **93**, 121103(R) (2016).
- ⁴³ A. Georges, G. Kotliar, W. Krauth, and M. J. Rozenberg, *Rev. Mod. Phys.* **68**, 13 (1996).
- ⁴⁴ A. Sekiyama, H. Fujiwara, S. Imada, S. Suga, H. Eisaki, S. I. Uchida, K. Takegahara, H. Harima, Y. Saitoh, I. A. Nekrasov, et al., *Phys. Rev. Lett.* **93**, 156402 (2004).
- ⁴⁵ F. Mazzola, V. Sunko, S. Khim, H. Rosner, P. Kushwaha, O. J. Clark, L. Bawden, I. Marković, T. K. Kim, M. Hoesch, et al., arXiv:1710.05392 (2017).
- ⁴⁶ L. Boehnke, A. I. Lichtenstein, M. I. Katsnelson, and F. Lechermann, arXiv:1407.4795 (2014).